The Effect of Nb Content on the Thermal, Structural, and Magnetic Properties of FeNbB Ribbons

Z. Hua*, B. Zuo, M.Y. Li, X.N. Wang, L.L. Wang, J. Liu, D. Wang and L.R. Dong
Key Laboratory of Functional Materials Physics and Chemistry of the Ministry of Education
Jilin Normal University, Siping 136000, Jilin, P.R. China

(Received May 8, 2013; in final form July 30, 2013)

Amorphous $Fe_{80-x}Nb_xB_{20}$ ($x = 5, 10, 15$) ribbons were prepared by single-roller melt spinning method. The thermal, structural and magnetic properties of $Fe_{80-x}Nb_xB_{20}$ ($x = 5, 10, 15$) ribbons were investigated using differential thermal analysis, X-ray diffraction, and vibrating sample magnetometer. The thermal stability is the lowest for $Fe_{70}Nb_{10}B_{20}$ ribbon and the highest for $Fe_{65}Nb_{15}B_{20}$ ribbon. Along with the increase of Nb content, the supercooled liquid region ΔT_x increases, indicating that the amorphous formation ability improves. The primary stages of crystallization of the three ribbons are different. The primary devitrification phases are $Fe_{23}B_6$ type for $Fe_{70}Nb_{10}B_{20}$ and $Fe_{75}Nb_5B_{20}$ ribbons, and α-Fe type for $Fe_{65}Nb_{15}B_{20}$ ribbon. $Fe_{80-x}Nb_xB_{20}$ ($x = 5, 10$) ribbons are ferromagnetic and the $Fe_{65}Nb_{15}B_{20}$ ribbon is paramagnetic. The saturation magnetization ($\boldsymbol{M}_s$) decreases with increasing Nb content.

DOI: 10.12693/APhysPolA.125.1149
PACS: 65.60.+a, 61.43.Dq

1. Introduction

Fe-based amorphous and nanocrystalline soft magnetic alloys have been widely studied over the last decade [1–10]. Fe-based ribbons have good soft magnetic properties and are widely used as the electromagnetic materials. Many investigations focus on the FeNbB alloys [6–10]. The crystallization behaviors [6], crystallization process [7], and magnetic property [8] of FeNbB alloys were studied.

Itoi and Inoue [9] have reported the effect of B content on thermal stability of Fe–Nb–B alloys. Stokłosa [10] reported the influence of boron content on crystallization and magnetic properties of ternary FeNbB amorphous alloys.

The purpose of this study is to investigate the effect of Nb content on the thermal, structural and magnetic properties of $Fe_{80-x}Nb_xB_{20}$ ($x = 5, 10, 15$) ribbons.

2. Experimental details

Amorphous ribbons of $Fe_{80-x}Nb_xB_{20}$ ($x = 5, 10, 15$) with 4 mm width and 30 μm thickness were obtained by the single-roller melt spinning technique at a surface velocity of 38 m/s. The microstructure was examined by X-ray diffraction (XRD, D/max 2500/PC, Cu K_α, $\lambda = 1.5406$ Å). The thermal analysis was investigated by differential thermal analysis (DTA, TG/DTA-6300). The magnetic property was performed by the vibrating sample magnetometer (VSM, Lake Shore M-7407).

*corresponding author; e-mail: huazhong196110@163.com

3. Results and discussion

Figure 1 shows the DTA curves of $Fe_{80-x}Nb_xB_{20}$ ($x = 5, 10, 15$) ribbons at different heating rates. The first crystallization peaks T_p of $Fe_{80-x}Nb_xB_{20}$ ($x = 5, 10, 15$) amorphous ribbons obtained at different heating rates are listed in Table I. T_p increases with the increase of Nb content. The increase of T_p should be related to the fact that Nb has higher melting temperature than Fe. The apparent activation energy of crystallization is calculated using the Kissinger equation [11], by plotting $\ln(\nu/T^2)$ versus $1/T$ (a straight line with the slope of E/R), where R is the gas constant, ν is the heating rate (K/min) and T is a specific absolute temperature such as crystallization peak T_p.

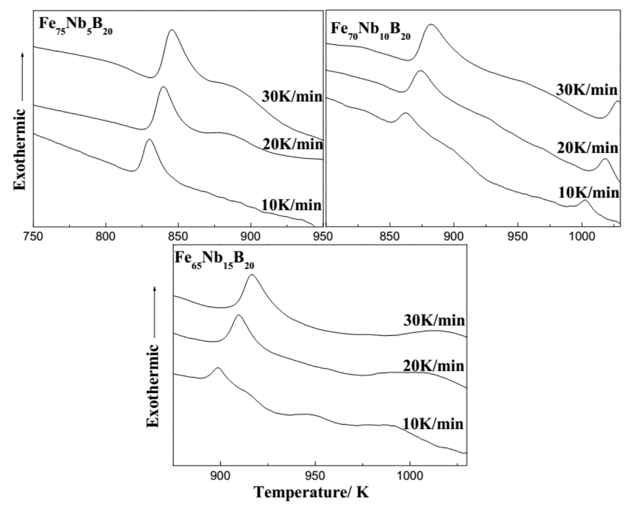

Fig. 1. DTA curves of $Fe_{80-x}Nb_xB_{20}$ ($x = 5, 10, 15$) ribbons at different heating rates.

TABLE I

The first crystallization peaks T_p of $Fe_{80-x}Nb_xB_{20}$ ($x = 5, 10, 15$) amorphous ribbons obtained at different heating rates.

ν [K/min]	T_P [K]		
	10	20	30
$Fe_{75}Nb_5B_{20}$	830.4	839.4	845.4
$Fe_{70}Nb_{10}B_{20}$	861.7	873.4	882.4
$Fe_{65}Nb_{15}B_{20}$	898.8	909.1	916.0

Figure 2 shows the Kissinger plots of $Fe_{80-x}Nb_xB_{20}$ ($x = 5, 10, 15$) ribbons for T_p; the apparent activation energies are 414.9, 323.0, and 425.7 kJ/mol, respectively. The thermal stability is the lowest for $Fe_{70}Nb_{10}B_{20}$ ribbon and the highest for $Fe_{65}Nb_{15}B_{20}$ ribbon.

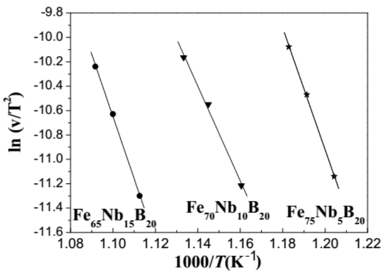

Fig. 2. Kissinger plots of $Fe_{80-x}Nb_xB_{20}$ ($x = 5, 10, 15$) ribbons for T_p.

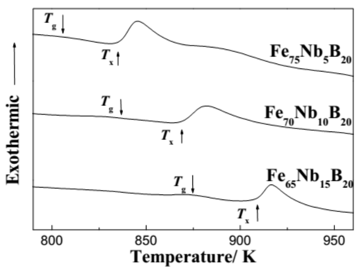

Fig. 3. DTA curves of $Fe_{80-x}Nb_xB_{20}$ ($x = 5, 10, 15$) amorphous ribbons at a heating rate of 30 K/min.

Figure 3 shows the DTA curves of $Fe_{80-x}Nb_xB_{20}$ ($x = 5, 10, 15$) amorphous ribbons at a heating rate of 30 K/min. T_g, T_x and ΔT_x of $Fe_{80-x}Nb_xB_{20}$ ($x = 5, 10, 15$) amorphous ribbons at a heating rate of 30 K/min are shown in Table II. Along with the increase of Nb content, the glass transition temperature T_g and the onset crystallization T_x shift towards high temperatures. Supercooled liquid region ΔT_x ($\Delta T_x = T_x - T_g$) increases gradually, indicating that the amorphous formation ability improves.

Figure 4 shows the XRD patterns of as-quenched and annealed $Fe_{80-x}Nb_xB_{20}$ ($x = 5, 10, 15$) ribbons. No crystalline peaks are observed in the XRD patterns of three as-quenched ribbons, which prove that the as-quenched

TABLE II

T_g, T_x and ΔT_x of $Fe_{80-x}Nb_xB_{20}$ ($x = 5, 10, 15$) amorphous ribbons at a heating rate of 30 K/min.

	T_g	T_x	ΔT_x
$Fe_{75}Nb_5B_{20}$	805.629	836.603	30.974
$Fe_{70}Nb_{10}B_{20}$	833.760	867.931	34.171
$Fe_{65}Nb_{15}B_{20}$	874.538	910.340	35.802

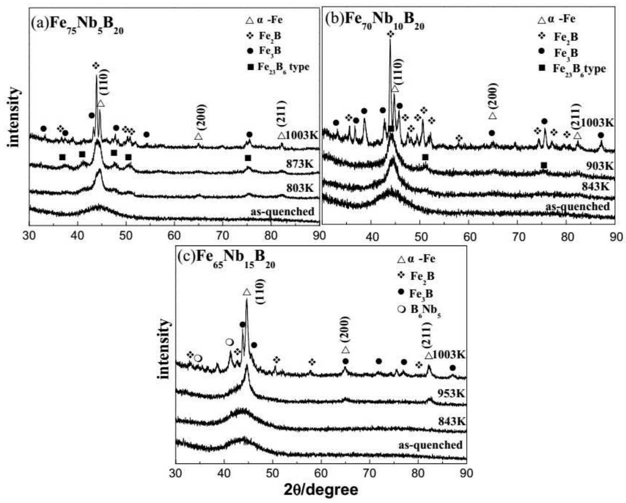

Fig. 4. XRD patterns of as-quenched and annealed $Fe_{80-x}Nb_xB_{20}$ ($x = 5, 10, 15$) ribbons.

ribbons are all amorphous. FeNbB system is favored in the three empirical rules [12]. FeNbB system consists of three components (Fe, Nb and B). There is significant difference in atomic size ratios above 12% among the main constituent elements and the sequence of atomic size is R_{Nb} (0.198 nm) $>$ R_{Fe} (0.156 nm) $>$ R_B (0.087 nm). The negative heats of mixing of Fe–B, Nb–Fe, and Nb–B are −26, −16 and −54 kJ/mol [13], respectively. This system has high negative heats of mixing.

The primary stage of crystallization of the three ribbons changes with Nb content addition. The primary devitrification phase of $Fe_{70}Nb_{10}B_{20}$ and $Fe_{75}Nb_5B_{20}$ are similar, which is the metastable phase of $Fe_{23}B_6$ type. It seems that the $Fe_{23}B_6$ type was formed by annealing at lower temperatures, 843 K for $Fe_{70}Nb_{10}B_{20}$ and 803 K for $Fe_{75}Nb_5B_{20}$, which coincides with the results of Imafuku et al. [14]. $Fe_{65}Nb_{15}B_{20}$ is still in amorphous state at 843 K, which is related to its high thermal stability. The primary devitrification phase of $Fe_{65}Nb_{15}B_{20}$ is very different from $Fe_{70}Nb_{10}B_{20}$ and $Fe_{75}Nb_5B_{20}$. The primary devitrification phase of the $Fe_{65}Nb_{15}B_{20}$ is α-Fe type crystalline phase.

Figure 5 shows the hysteresis loops of as-quenched $Fe_{80-x}Nb_xB_{20}$ ($x = 5, 10, 15$) ribbons at room--temperature. $Fe_{80-x}Nb_xB_{20}$ ($x = 5, 10$) ribbons are ferromagnetic and $Fe_{65}Nb_{15}B_{20}$ ribbon is paramagnetic. The inset shows the M–T curve of $Fe_{65}Nb_{15}B_{20}$ ribbon at low temperature. The Curie temperature of $Fe_{65}Nb_{15}B_{20}$

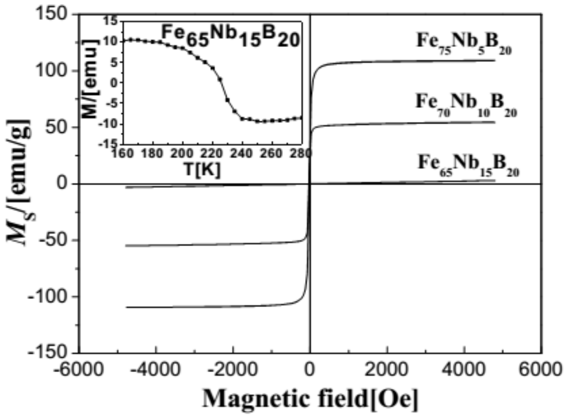

Fig. 5. The hysteresis loops of $Fe_{80-x}Nb_xB_{20}$ ($x = 5, 10, 15$) ribbons as-quenched at room temperature. The inset shows the M–T curve of $Fe_{65}Nb_{15}B_{20}$ ribbon at low temperature.

ribbon is 225 K. The saturation magnetization ($\boldsymbol{M}_s$) decreases with increasing Nb content. The variation can be related to the variation in the magnetic moment. On the one hand, due to the Fe substitution for Nb, the Fe content decreases, so the magnetic moment of sample decreases. On the other hand, the variation of $\boldsymbol{M}_s$ is related to the competition between ferromagnetic and antiferromagnetic exchange interaction. Antiferromagnetic coupling was formed between Fe and Nb [15]. Antiferromagnetic exchange interaction increases and ferromagnetic exchange interaction decreases with increasing Nb content, so $\boldsymbol{M}_s$ decreases [16].

4. Conclusions

(1) The apparent activation energies of the $Fe_{80-x}Nb_xB_{20}$ ($x = 5, 10, 15$) ribbons are 414.9, 323.0, and 425.7 kJ/mol, respectively. The thermal stability is the lowest for $Fe_{70}Nb_{10}B_{20}$ ribbon and the highest for $Fe_{65}Nb_{15}B_{20}$ ribbon. Along with the increase of Nb content, the supercooled liquid region ΔT_x ($\Delta T_x = T_x - T_g$) increases gradually, indicating that the amorphous formation ability improves.

(2) The primary devitrification phase is metastable $Fe_{23}B_6$ type for $Fe_{70}Nb_{10}B_{20}$ and $Fe_{75}Nb_5B_{20}$ ribbons, which is formed by annealing at low temperatures: 843 K for $Fe_{70}Nb_{10}B_{20}$ ribbon and 803 K for $Fe_{75}Nb_5B_{20}$ ribbon. $Fe_{65}Nb_{15}B_{20}$ ribbon is still in the amorphous state at 843 K, which is related to its high thermal stability. The primary devitrification phase is α-Fe type for the $Fe_{65}Nb_{15}B_{20}$ ribbon.

(3) $Fe_{80-x}Nb_xB_{20}$ ($x = 5, 10$) ribbons are ferromagnetic and the $Fe_{65}Nb_{15}B_{20}$ ribbon is paramagnetic. The saturation magnetization ($\boldsymbol{M}_s$) decreases with increasing Nb content, which is related to the magnetic moment.

Acknowledgments

This work was funded by Science and Technology Development Project of Jilin Province (No. 201105083), Science and Technology Studying Project of "12th five-year" Office of Education of Jilin Province (No. 2011-158) and Graduate Innovative Research Programs of Jilin Normal University (No. 201103).

References

[1] W.Q. Yu, Y.M. Sun, L.H. Liu, L.R. Dong, Z. Hua, *Acta Phys. Pol. A* **120**, 1034 (2011).
[2] A. Baron, D. Szewieczek, G. Nawrat, *Electrochim. Acta* **52**, 5690 (2007).
[3] T. Tokunaga, K. Terashima, H. Ohtani, M. Hasebe *Mater. Trans.* **49**, 2534 (2008).
[4] T. Tamura, D. Kamikihara, Y. Mizutani, K. Miwa, *Mater. Trans.* **47**, 1360 (2006).
[5] H. Huang, G. Shao, P. Tsakiropoulos, *J. Alloys Comp.* **459**, 185 (2008).
[6] M. Imafuku, S. Sato, H. Koshiba, E. Matsubara, A. Inoue, *Mater. Trans. JIM* **41**, 1526 (2000).
[7] J. Torrens-Serra, P. Bruna, J. Rodríguez-Viejo, T. Pradell, M.T. Clavaguera-Mora, *Rev. Adv. Mater. Sci.* **18**, 464 (2008).
[8] Y.H. Gao, D. Shindo, *Phys. Rev. B* **67**, 172409 (2003).
[9] T. Itoi, A. Inoue, *Mater. Trans. JIM* **40**, 643 (1999).
[10] Z. Stokłosa, J. Rasek, *Phys. Status Solidi A* **207**, 452 (2010).
[11] H.E. Kissinger, *Anal. Chem.* **29**, 1702 (1957).
[12] A. Inoue, A. Takeuchi, T. Zhang, *Metall. Mater. Trans. A* **29**, 1779 (1998).
[13] A. Takeuchi, A. Inoue, *Mater. Trans.* **46**, 2817 (2005).
[14] M. Imafuku, S. Sato, H. Koshiba, E. Matsubara, A. Inoue, *Scr. Mater.* **44**, 2369 (2001).
[15] W.S. Zhan, B.G. Shen, J.G. Zhao, *Acta Phys. Sin.* **34**, 1613 (1985).
[16] Y. Hu, L. Liu, K.C. Chan, M.X. Pan, W.H. Wang, *Mater. Lett.* **60**, 1080 (2006).